Final Report:

Methane, Ethane, and Propane Sensor for Real-time Leak Detection and Diagnostics

Department of Energy

Office of Fossil Energy

SBIR Phase I Release 2

Topic 19b

Award No. DE-SC0015736

Aerodyne Research, Inc.

Principal Investigator:

Joseph R. Roscioli

Co-investigators:

Scott C. Herndon
David D. Nelson
Tara I. Yacovitch

Report # DOE-ARI-11219-1

March 24, 2017

Executive Summary

The Phase I effort demonstrated the technical viability of a fast, sensitive, mobile hydrocarbon monitor. The instrument will enable the oil and gas industry, researchers, and regulators to rapidly identify and chemically profile leaks from facilities. This capability will allow operators to quickly narrow down and mitigate probable leaking equipment, minimizing product loss and penalties due to regulatory non-compliance. During the initial development phase, we demonstrated operation of a prototype monitor that is capable of measuring methane, ethane, and propane at sub-part-per-billion sensitivities in 1 second, using direct absorption infrared spectroscopy. To our knowledge, *this is the first instrument capable of fast propane measurements at atmospheric concentrations*. In addition, the electrical requirements of the monitor have been reduced from the 1,200 W typical of a spectrometer, to <500 W, making it capable of being powered by a passenger vehicle, and easily deployed by the industry.

The prototype monitor leverages recent advances in laser technology, using high-efficiency interband cascade lasers to access the 3 µm region of the mid-infrared, where the methane, ethane, and propane absorptions are strongest. Combined with established spectrometer technology, we have achieved precisions noted in the inset table. This allows the monitor to measure fast plumes from oil and gas facilities, as well as ambient background concentrations (typical ambient levels are 2 ppm, 1.5 ppb, and 0.7 ppb for methane, ethane and propane, respectively). Increases in instrument operating pressure were studied in order to allow for a smaller 125 W pump to be used, and passive cooling was explored to reduce the cooling load by almost 90% relative to active (refrigerated) cooling. In addition, the simulated infrared absorption profiles of ethane and propane were modified to minimize crosstalk between species, achieving <1% crosstalk between ethane and propane. Finally, a monitor was designed based upon the commercial compact mini-spectrometer capable of dual-laser operation. We intend to build and test this during phase II.

Gas Species	Sensitivity (2s)
CH_4, methane	104 pptv
C_2H_6, ethane	23 pptv
C_3H_8, propane	74 pptv

Multiple opportunities for improvement were also identified. First, the reported ethane and propane concentrations are susceptible to external acceleration acting upon the instrument. During phase II we will address this “motion-sickness”. Second, significant software development will be needed operate the monitor at 1 second resolution in real time, and provide rapid, actionable data to a driver or passenger.

Introduction

The U.S. oil and gas industry has recently experienced an economic boom due to the advent of novel methods for accessing shale and tight gas plays.[1] With this increased production comes the need to identify and assess possible environmental and economic consequences associated with emissions of upstream oil and gas activities. From an industry operations perspective, locating and fixing leaks will reduce product losses, improve safety, and minimize penalties due to non-compliance. From an environmental perspective, methane (CH_4), the primary component of natural gas, is a potent greenhouse gas with a 100-year global warming potential 25 times that of CO_2.[2] The International Energy Agency has recently stated that "reducing *methane emissions* in oil and gas production" is a key component of their "Bridge" strategy that will peak global energy related emissions by 2020.[3]

Identifying and quantifying these emissions has become a major research and industry objective over the past 25 years.[4-7] The quantification of CH_4 from such infrastructure is complicated by the sheer number of possible leak points at a typical facility, and the difficulty of accessing them for analysis. In addition to the hundreds of miles of pipeline, the journey from one of 515,000 wells nationwide to an end user includes passing through compressors, exposure to thousands of high pressure components such as valves and seals, dumping to produced water and condensate tanks, and processing in dehydrators, amine reactors, and distillation stacks.

Existing leak detection and repair (LDAR) technology requires either significant mobile laboratory infrastructure, or significant manpower, or lacks the ability to identify probable leak locations at a large O&G facility. Recent field measurements of downwind plumes from natural gas leaks have found that the chemical signatures of accompanying compounds can indicate the locations of these leaks.[8] In particular, ethane and propane are frequently co-emitted with methane, and can be used to identify the specific equipment responsible for a downwind plume. We have previously demonstrated rapid measurements of ethane and methane with high sensitivity using high resolution infrared spectroscopy.[9] The primary result of the phase I effort reported here is a prototype methane, ethane, and propane sensor based upon a tunable infrared laser direct absorption spectrometer (TILDAS), that is fast (2-second), sensitive (<1 ppb), and has a small electrical and spatial footprint. This will allow the sensor to be operated from inside a passenger vehicle or pickup truck, with little technical expertise required. The intended application is for deployment aboard fleet vehicles during existing regular maintenance activities at gas facilities, or as part of a dedicated leak surveys operated by either the industry or academic/environmental organizations.

Scientific and Technical Results

The major accomplishments from this effort are:

1) *Implementation of dual laser approach to detect methane, ethane and propane simultaneously*
2) *Minimized spectral crosstalk to <1% between all three species*
3) *Demonstrated 1-second sensitivities of 100 ppt, 25 ppt, and 75 ppt on CH_4, C_2H_6, and C_3H_8, respectively*
4) *Illustrated capabilities for laboratory deployment (roof-sampling) and mobile deployment (oil and gas field in Alberta, Canada)*
5) *Reduced pumping power consumption to <150 W and cooling consumption to <50 W*
6) *Designed phase II instrument to make use of the dual-mini TILDAS chassis – 19" rack-mountable and <10"' tall*

This project consisted of 4 primary tasks aimed at developing and testing technology towards a compact, fast, and precise methane/ethane/propane detection:

I. Spectral Simulations: Determine the optimal spectral regions to probe methane, ethane, and propane in the mid-infrared, and identify issues with spectral interferences and pressure broadening.
II. Demonstration and Testing: Set up tunable infrared laser direct absorption spectrometer (TILDAS) with both lasers, determine noise levels, quantify and mitigate interferences. Calibrate signals against a standard. Demonstrate in laboratory and mobile setting.
III. Power/Size Reduction: Reduce power consumption using passive cooling and a smaller pump. Explore other packaging options to minimize spatial footprint.
IV. Design Phase II Instrument: Integrate results from previous 3 tasks to design compact, precise instrument to build during phase II.

Detailed technical results and accomplishments from each task are described below.

Task I: Spectral Simulations

The central goals of task I were to establish the spectroscopy needed to accurately and precisely quantify the species of interest. This was broken into several sub-parts, described below.

1) Explore spectral simulations to determine the optimal wavelengths to detect CH_4, C_2H_6, and C_3H_8.
2) Purchase and characterize the required lasers
3) Identify the possible interferences

4) Consider the effects of pressure broadening to see if higher operating pressures were reasonable

1) Explore spectral simulations to determine the optimal wavelengths to detect CH_4, C_2H_6, and C_3H_8

During this part, the spectral signatures of all three species were identified and simulated. In order to minimize the need for an extensive cooling footprint (described in Task III), we restricted our search to the mid-infrared 3 µm region, corresponding to the C-H stretch molecular vibrations. Although the methane spectrum is very well understood in this region, a detailed quantification of ethane and propane absorptions has only recently been performed by Harrison and coworkers.[10, 11] Figure 1 shows simulated spectra for 2 ppm of CH_4, 10 ppb of C_2H_6, and 10 ppb of C_3H_8 in the 2950-3020 cm^{-1} region. The methane simulation is based upon the HITRAN database,[12] while the ethane and propane features are based upon the work by Harrison and Bernath. The blue shaded region near 2990 cm^{-1} has strong methane and ethane features, while the pink region near 2967 cm^{-1} has the only large propane feature as well as a strong methane line. Between these two scan regions, the C_1-C_3 species can be quantified.

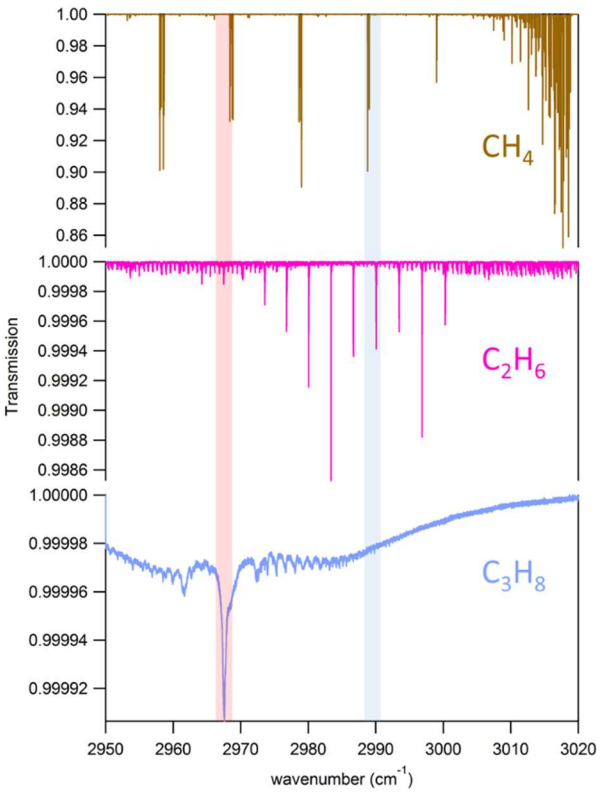

Figure 1. Two spectral regions to detect methane, ethane (2990 cm^{-1}, and propane (2967 cm^{-1})

Notably, the 2967 cm^{-1} region still has distinct ethane absorptions, ~5x smaller than that at 2990 cm^{-1}, but nearly overlapping with the broad propane feature. This is shown more clearly in Figure 2. The peak positions of C_2H_6 and C_3H_8 are 0.06 cm^{-1} apart, and because of their widths, the majority of the C_2H_6 peak is enveloped by the C_3H_8. In addition, the line depths of the species are comparable (~10^{-4} absorbance for 10 ppb). This implies that there is the potential for significant crosstalk between the two species if they are both measured near 2967 cm^{-1}. This crosstalk will be quantified in Task II, but the best way to mitigate it is to independently measure ethane in a different spectral region (2990 cm^{-1}), and apply that measured concentration to the ethane absorption at 2967 cm^{-1}.

2) Purchase and characterize the required lasers

Interband cascade lasers (ICLs) have been recently developed to operate in the 3 µm region.[13, 14] These light sources are high resolution ($\Delta\nu$ < 0.001 cm^{-1}), and highly efficient – typical emissions are >2 mW, require <50 mA to lase, and operate at near room temperature. These characteristics are summarized in Table 1. The lasers were tested to make sure they were not multimode (operating at multiple frequencies) by exposing TILDAS to high ethane and methane concentrations, where the absorptions should be optically dark. If the line centers fully absorb light through the multipass cell, the laser is not multimode.

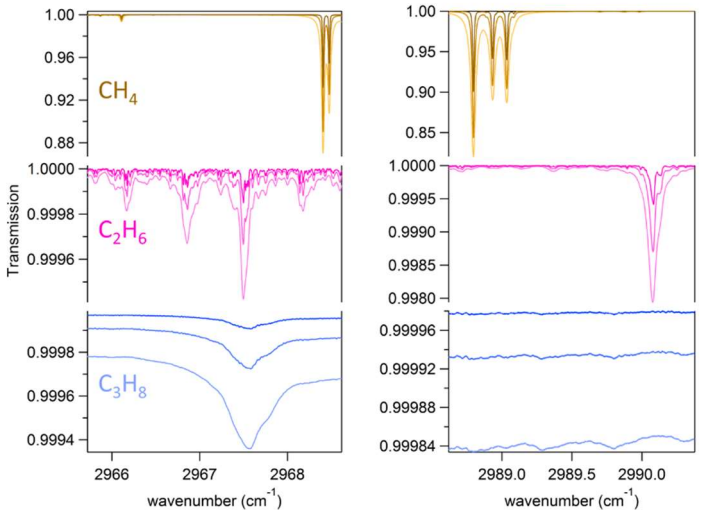

Figure 2. Detailed spectral simulation of 2967 cm^{-1} region for propane, and 2990 cm^{-1} for ethane and methane. The spectra are simulated for 3 different absorption cell pressures: 30, 90, and 215 Torr, in order of darkest to lightest.

Table 1. Interband Cascade Laser (ICL) operating conditions

Frequency	Power	Operating Current	Operating Temperature
2990	>1	15	8
2967	>3	40	35

3) Identify possible spectral interferences

Finally, the 2967 cm^{-1} laser needs to scan an extended range, to cover the propane absorption. This is complicated by the presence of water at lower frequency and methane at higher frequency, as shown in Figure 3. These strong transitions determine the bounds of the propane fit, since including them in the fit will induce relatively large biases in the propane mixing ratio. As such, the scan must cover 2966.0 – 2968.5 cm^{-1}, a 2.5 cm^{-1} range. The laser was actually found to operate across nearly 2.8 cm^{-1}. Meanwhile, the 2990 cm^{-1} laser operates across 1.5 cm^{-1} to cover both the methane and ethane absorptions.

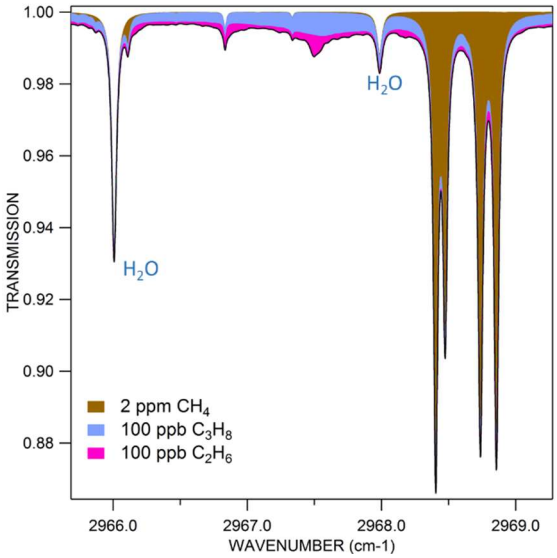

Figure 3. Water lines (transparent), along with 2 ppm CH_4, 100 ppb C_2H_6, and 100 ppb of C_3H_8.

4) Determine effect of elevated pressure

TILDAS instruments typically operate best at low cell pressures between 20 and 60 Torr. The reason for this is shown in Figure 4. Increases in

pressure result in pressure-broadening of the sharp CH_4 line by a factor of >10 in going from 30 to 760 Torr. However, the line depth, which largely defines the sensitivity of the TILDAS, only increases by a factor of <2. Because the extra width frequently comes at the cost of increased crosstalk between peaks, <100 Torr is the preferred operating cell pressure. However, this preference changes for absorption profiles whose widths are defined by factors other than pressure. In the case of propane and ethane the absorption feature is a composite of many underlying transitions, where the width is due to the multitude of frequencies of those transitions. As seen in Figure 4, for these species the fractional increase in width is <4 when increasing the pressure from 30 to 760 Torr, but the line depths increase significantly. This is especially true for propane: the width increases by a factor of 1.4, but the line depth increases by a factor of 20. This makes pressure increases beneficial to sensitivity for ethane and propane. During Task II we will discuss the practical implications of such an increase.

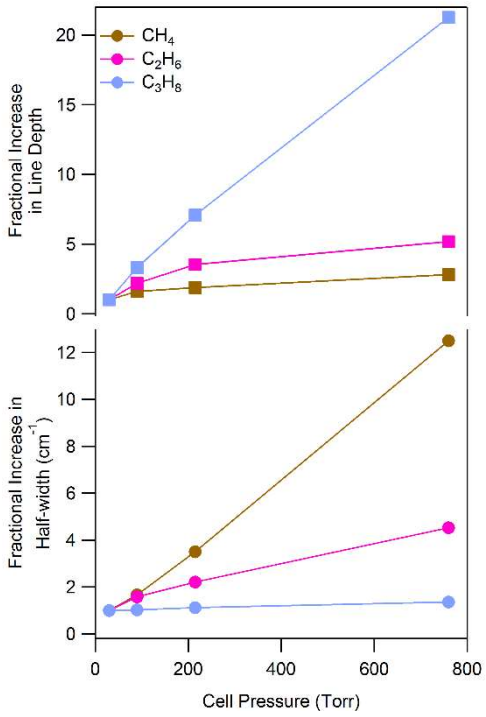

Figure 4. Increase in width (lower trace) and line depth (upper trace) for methane (brown), ethane (pink) and propane (blue) as a function of absorption cell pressure.

Task II: Laboratory Demonstration and Testing

During the phase I testing, a dual-laser TILDAS was used to quantify not only sensitivity on methane, ethane, and propane, but also interferences with other species.[15] This is particularly relevant to the propane measurements, where the propane spectrum is particularly broad, overlapping with water, ethane, methane, ethylene, and methanol absorptions. During this task, we performed the following testing:

1) Raw C_1-C_3 sensitivity
2) Quantifying and minimizing cross-talk between ethane, water, and propane
3) Calibration of the C_1-C_3 measurements
4) Reduction of the influence of water to the C_1-C_3 measurements
5) Field testing of the instrument in a stationary environment (sampling from Aerodyne roof) and
6) Field testing aboard a mobile platform (the Aerodyne Miniature Mobile Laboratory, minAML)

All testing was performed on a dual-TILDAS with a 76 meter absorption cell.

1) Raw C_1-C_3 sensitivity

After determining the optimal wavelength(s) for C_1-C_3 detection and acquiring the correct lasers (Task I), the first test of interest is to determine the sensitivity of the instrument to these compounds. This was determined via sampling a re-humidified gas flow from a stable compressed air cylinder that contained ambient levels of CH_4, C_2H_6, C_3H_8. Shown in Figure 5, Figure 6, and Figure 7 are the noise characteristic of a dual instrument operating with laser 1 at 2990 cm^{-1} and laser 2 at 2967 cm^{-1}. During these tests, the fastest measurement was performed at 2 second intervals, limited primarily by the acquisition computer's ability to fit absorptions of 12 species at once. During phase II, we will explore using faster processing computers and modification of existing software to take advantage of multiple-core processors.

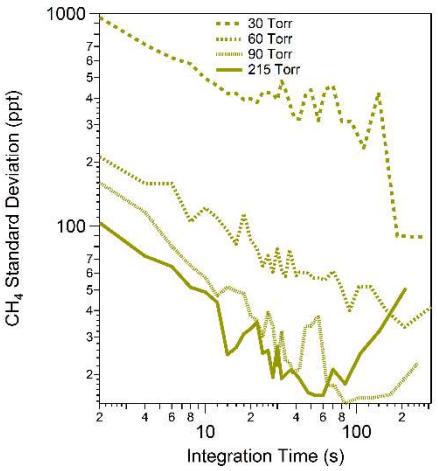

Figure 5. Standard deviation of CH_4 measurement as a function of averaging time.

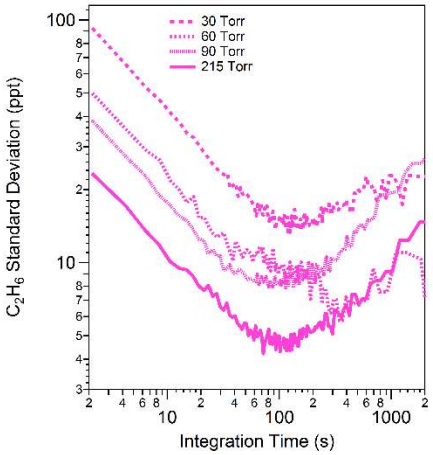

Figure 6. Standard deviation of C_2H_6 measurement as a function of averaging time.

As can be seen in Figures 5-7, and summarized in Table 2, the noise levels of methane, ethane, and propane are dependent upon cell pressure. This is not surprising, given that a higher cell pressure corresponds to a higher number density and stronger infrared absorptions for a given cross-section, as discussed in Task I. On one hand, increasing the cell pressure improves sensitivity. On the other hand, that increase in pressure broadens the transitions and can lead to introduction of other noise sources such as crosstalk between species. That trade-off typically occurs near in the 30-60 Torr range, so a TILDAS usually operates at a cell pressure of 30-50 Torr. This is demonstrated in Figure 5 for methane, where there may be significant improvement in going from 30 to 60 Torr, but not much improvement beyond that. A discussed above, the ethane and propane measurements are an exception to that rule since their infrared absorptions are already broadened by the presence of many rovibrational transitions contributing to a single infrared "peak", so pressure-broadening does not significantly widen those peaks. The trade-off, however, is in inlet flow – to achieve the same volumetric time response, the inlet flow must be higher for higher pressures, requiring a pump that can manage such a flow.

Table 2. Measured noise for methane, ethane and propane at short and long timescales, at an operating pressure of 215 Torr.

Species	2 second noise (ppt)	100 second noise (ppt)
CH_4	104	25
C_2H_6	23	4
C_3H_8	74	43

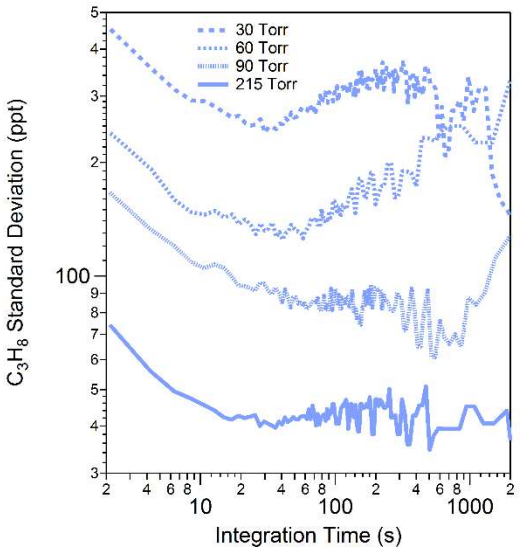

Figure 7. Standard deviation of C_3H_8 measurement as a function of averaging time.

The ethane and methane sensitivities observed here are similar to what we have observed in the past: 20-100 ppt for ethane and 100-1000 ppt for methane. For propane, these are the first fast-response quantifications of a propane TILDAS, and demonstrate a noise level of <500 ppt in 2 seconds. At the highest cell pressure (215 Torr), the 2-s noise was 74 ppt. For reference, the 2-s dark noise for each species is 12, 7, and 24 ppt for CH_4, C_2H_6 and C_3H_8, respectively at a cell pressure of 215 Torr. In addition, all three measurements average down considerably over long term, at all pressures. At 100 s and 215 Torr, the noise levels are 25 ppt, 5 ppt, and 43 ppt for methane, ethane, and propane, respectively. It should be noted that in this testing, a 76 meter absorption cell was employed. If a larger cell (available only in a dual-TILDAS spectrometer) were used, the path length could be increased to as much as 400 m. In such a case, the 2-s noise would be as low as 20, 4, and 14 ppt, respectively. Long term 100-s noise would be 5, 1, and 8 ppt, respectively. As a point of comparison, the gas chromatograph-based NOAA Global Monitoring Division measurements of ethane and propane have reported sensitivities of 3 and 2 ppt, respectively. The long-term sensitivities with a 400 meter absorption cell would therefore be competitive with GC methods for long term quantification. The proposed instrument is valuable to not only plume measurement applications, but also ambient atmospheric sampling, such as those performed at tower and roof sampling locations worldwide.

2) Quantifying and minimizing cross-talk between ethane, water, and propane

Because the propane and ethane lines are both broad, there is potential for significant crosstalk between these channels in the 2967 cm^{-1} range. For the intended application of this instrument, minimizing this crosstalk is critical, as the propane/methane, propane/ethane, and ethane/methane ratios are important to standoff leak identification.

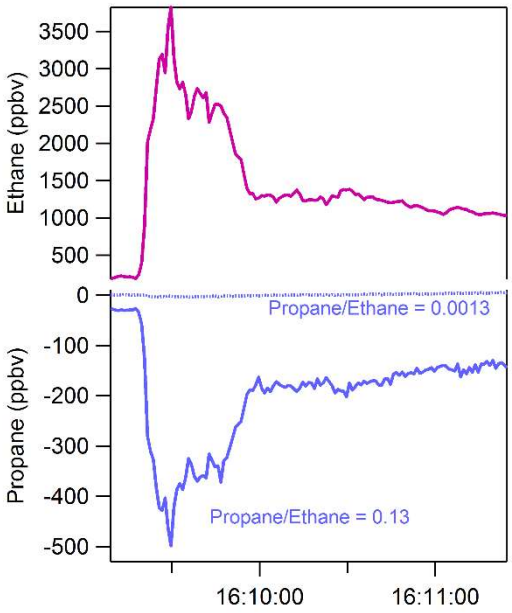

Figure 8. Quantification of ethane-propane crosstalk due to injection of ethane into laboratory. Solid blue line: crossstalk when using un-optimized propane and ethane simulation file. Dotted blue line: crosstalk when using optimized simulation files.

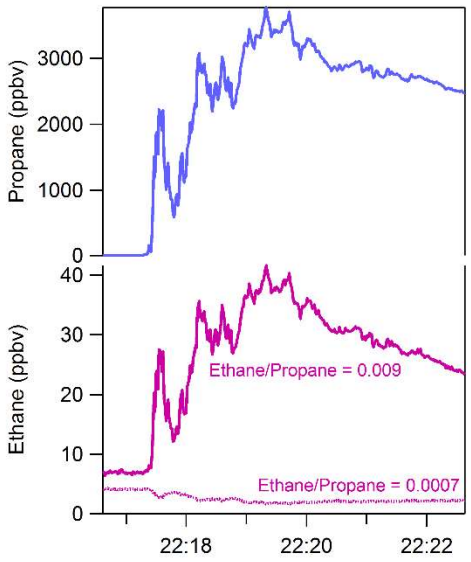

Figure 9. Ethane-propane crosstalk due to injection of propane into the laboratory. Solid pink line: crosstalk when using un-optimized propane and ethane simulation file. Dotted pink line: crosstalk when using optimized simulation files.

To test this, a small amount of pure ethane (~ 1 L) was released into the laboratory from which the instrument was sampling while the propane concentration was monitored, and vice versa. All measurements described below were using a 90 Torr cell pressure. It is unclear what the cross-talk dependence would be at higher or lower pressures, given how broad the ethane and methane absorptions already are.

Shown in Figure 8 is the response of propane to a surge of ethane in the laboratory. Using an approximate fit of the propane and ethane lineshapes results in a crosstalk of 13% (0.13, solid blue line). These approximate fits are used initially because they allow for faster (2 second) fitting of the absorption profile in real time. When the recorded spectra were fit offline using a modified simulation that improved the fit residuals, the crosstalk was reduced by a factor of 100 to 0.13% (0.0013). Likewise, when a surge of propane is released in the room, as shown in Figure 9, the crosstalk is reduced from 0.9% to 0.07% when employing a more sophisticated fit lineshapes.

These results have two implications: first, the ratios of ethane and propane are highly sensitive to the fit model. As a case in point, if the lower-quality lineshapes are used, an observed ethane-to-methane ratio of several percent, which could be commonly observed in the field, would be dominated by a crosstalk of 0.13. As such, reducing the effect to <1% is important. Second, the while the enhanced fit lineshape has produced better results, it is computationally intensive. To observe the fit mixing ratios on the fly using the more accurate lineshapes, the instrument needs to run at <0.5 Hz (>2 second time intervals). Alternatively, the instrument may run at a faster rate (up to 10 Hz), but the data will have to be re-analyzed using the improved simulations on a high-performance platform. During phase II, we will explore more robust computing options, including using faster processors and taking advantage of multiple-core processors to dedicate one processor to data acquisition, and one to data analysis (fitting).

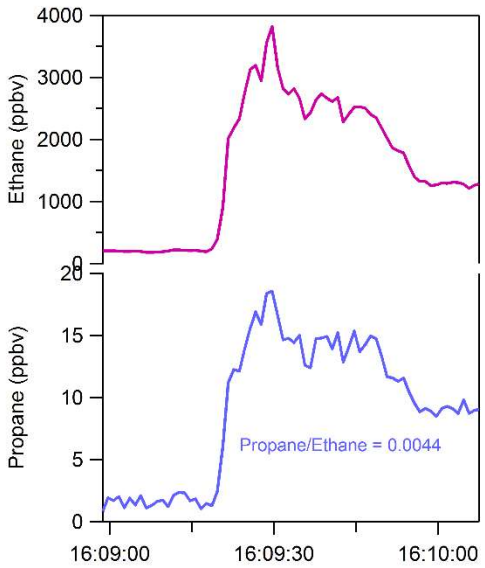

Figure 10. Ethane-propane crosstalk when the ethane is not measured independently in the 2990 cm^{-1} laser.

Finally, it should be noted that the 2967 cm^{-1} laser is capable of quantifying methane, ethane, and propane, but the ethane and propane absorptions are heavily overlapped (see Figure 2). Figure 10 shows the same ethane surge as in Figure 8, but the ethane concentration is floated in the 2967 cm^{-1} fit. This results in a propane/ethane crosstalk of 0.44% and an ethane mixing ratio noise of 120 ppt at 90 Torr (as opposed to 40 ppt using the 2990 cm^{-1} absorption). This demonstrates the value of independently measuring ethane and applying that independent value to the fit of ethane at 2967 cm^{-1}.

3) Calibration of the C_1-C_3 measurements

Calibrations of the propane instrument were carried out by quantitative dilution of a high-concentration standard (calibration tank) with hydrocarbon-free air ("zero air"). Mass-flow controllers were used to set flows of calibration and diluent gases.

The calibration tank was certified by the vendor to contain:

Component	Tank Certified (ppm)
Methane	50.1 ± 5%
Ethane	5.0 ± 5%
Propane	2.7 ± 5%
Air	balance

The TILDAS-dual propane instrument was operated at 86.6 Torr. Spectral simulations were performed live with a heavily culled set of absorption lines. Post-analysis was updated to use the improved propane simulation. The time series in Figure 11 shows the results of this post-analysis.

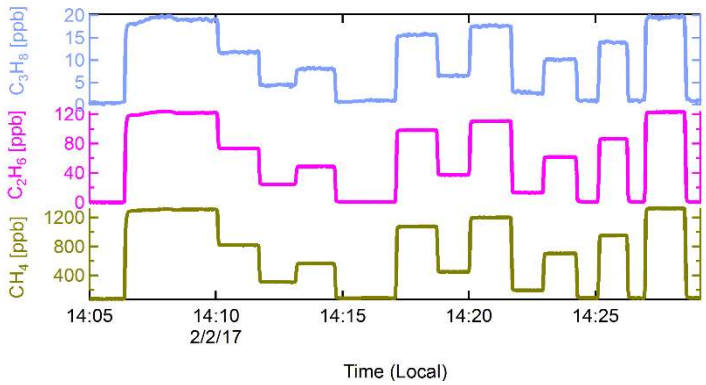

Figure 11. Time series of calibration of methane (yellow), ethane (red) and propane (blue).

Two other instruments measuring ethane and methane were hooked up in parallel to the C_1-C_3 prototype. An ethane mini-TILDAS (25 Torr cell pressure) and CH_4/N_2O mini-TILDAS provided auxiliary measurements of ethane and methane, respectively. These instruments give an independent measure of the accuracy of the calibration tank contents, discussed later on.

The results of the propane calibration are shown in Figure 12. Results pre- and post-refitting (circles and triangles) are shown. The real-time data analysis using the approximate hit files gives a first estimate of the propane measurement, but will depend strongly on the ethane

concentration. For this reason, the calibration factor of 0.496 retrieved for the fast hit files is not reliable. An ethane-only calibration could be performed to quantify the level of ethane interference in this fit. After refitting with the full spectral line set, the propane calibration factor of 0.282 is about 1/3 of what it should be. This implies that the line intensities in the propane hit file should be increased by a factor of 3.55. The calibration factor for ethane is 0.999, and for methane is 1.01.

One important result from these calibrations is that the retrieved mixing ratio is linear with propane concentration, with an excellent R^2. This means that the instrument can be easily calibrated with a single calibration factor. This persists over much larger concentration ranges.

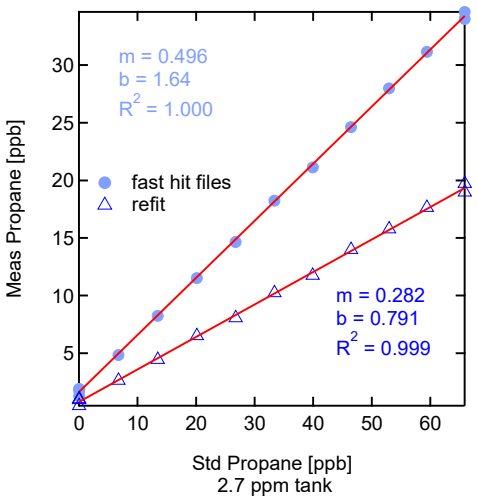

Figure 12. Propane calibration fit using un-optimized simulation files (solid dots) and optimized simulations (unfilled triangles), based upon calibration dilution standard.

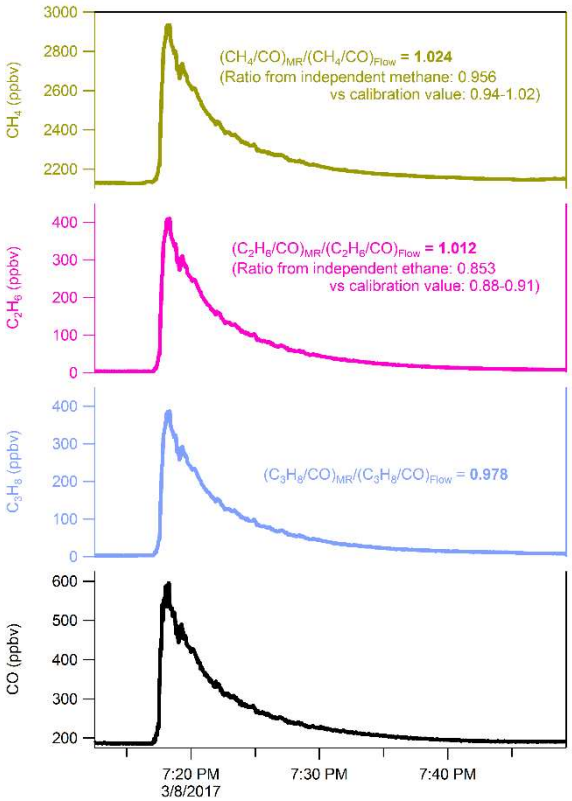

Figure 13. Secondary calibration approach, referencing the calibration factors of C_1-C_3 against a well-known CO calibration factor of 1.00.

The calibration factor of 3.55 is surprising, given that the other calibration factors are so close to unity. To test if the observed calibration factor was truly a function of the instrument or of an incorrectly prepared calibration cylinder, a different method was employed. Cylinders of pure (>99%) methane, ethane, propane, and carbon monoxide were fitted with mass flow controllers. Small, controlled flows (50 sccm for C_2H_6, C_3H_8, and CO; 100 sccm for CH_4) of each were combined and simultaneously released into the laboratory for 1 minute. This resulted in ~400 ppb increases in the ambient levels in the room, which slowly decayed back to ambient levels as the room ventilation cycled the air. The carbon monoxide measurement, using a separate mini-TILDAS, was independently calibrated against a known, certified standard, and was found to have a calibration factor of 1.00. It therefore served as the reference against which the C_1-C_3 measurements could compare. The calibration factor for methane, for example, could then be described by:

$$CH_4\ Cal.Factor = \frac{(\frac{CH_4}{CO})_{MR}}{(\frac{CH_4}{CO})_{flow}}$$

The results of this approach are shown in Figure 13. The enhancements and decays of all 4 species are very highly correlated, with R^2 values all >0.999. In this case, all calibration values are very near unity: 1.024, 1.012, and 0.978 for CH_4, C_2H_6, and C_3H_8, respectively. We therefore suspect that the existing C_1-C_3 calibration tank was not correctly prepared.

4) Reduction of the influence of water to the C_1-C_3 measurements

As can be seen in Task I, the impact of water may be important to the quantification of propane due to the sheer intensity of the H_2O line within 0.5 cm^{-1}. One way to minimize its impact is to stop fitting the propane spectrum before 2967.95 cm^{-1}, excluding the main intensity of the water line from the fit. While this certainly would mitigate the impact of the transition, the tail of the lineshape nonetheless plays an important role in the propane fit. We can instead reduce the effect by physically removing water from the sample stream. To achieve this, we employ a Nafion multi-tube (PD-100T-24MPS, PermaPure, LLC), which is capable of reducing water concentrations to dew points < -15 °C at a typical 3 SLPM flow rate.[16] Importantly, the dryer has *no disposable components and does not need regeneration.* This means it is a simple, permanent solution to removing water.

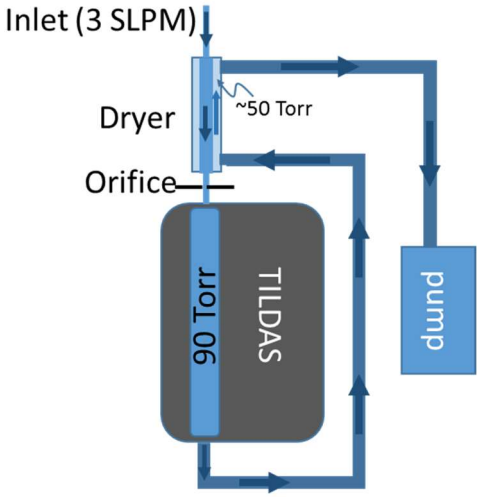

Figure 14. Flow schematic of drying nafion system. Inlet air passes through the nafion, where it is dried, the pressure is dropped, and then passes into the TILDAS. The sample air then passed thorugh the outer sheath of the nafion to dry the incoming air sample. This is also known as the "'reflux" method.

We confirmed the commercial dryer performance in the laboratory, finding a room temperature water concentrations of <0.08% (dew point -20 °C). The above noise and crosstalk analyses were performed using this Nafion pre-drying scheme. Figure 14 shows the pumping scheme to scrub water using the dryer. Based upon the principle of operation, the outer sheath of the dryer (pale blue in Figure 14) must either be at reduced pressure or have dry air passed through it, in order to have a water concentration gradient across the Nafion membrane. This is achieved by operating the dryer in "reflux" mode, where the sample that has run through the instrument is then passed through the outer sheath of the dryer ≪1 atmosphere. In this case, a critical orifice forces the pressure drop in the instrument (to ~90 Torr), after which the sample runs into the dryer sheath (now at ~50 Torr), before being drawing into the pump.

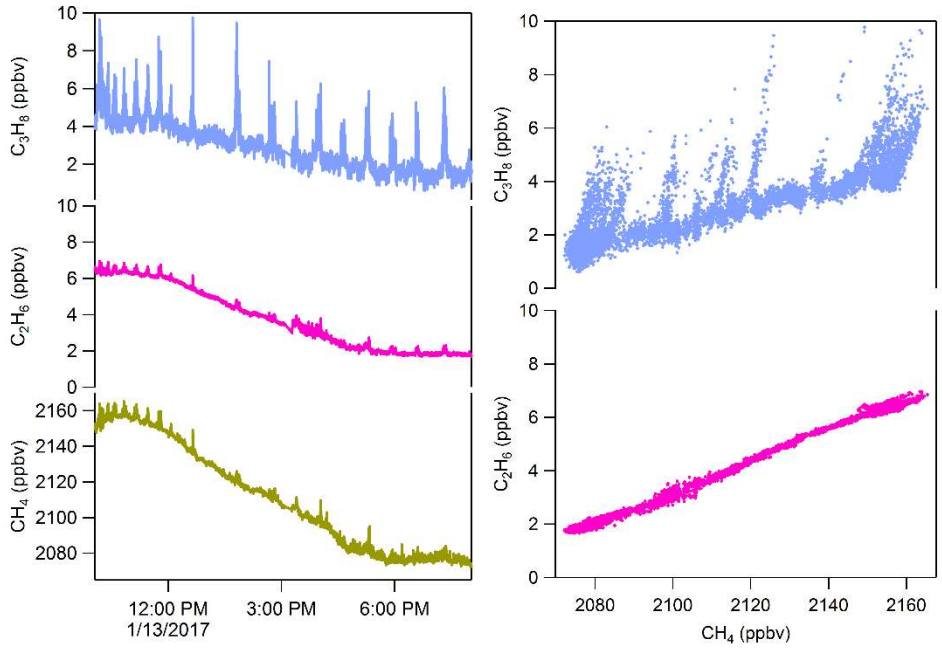

Figure 15. Left: exemplary high precision C_1-C_3 measurements from Aerodyne roof. Note the broad C_1-C_3 enhancement puctuated with fast, high-propane plumes. Right: correlation plots from this time series, showing very different correlations between the fast and slow propane enhancements.

There is a second benefit of the Nafion dryer. As opposed to other scrubbing technologies that remove a certain *fraction* of inlet water content, the Nafion achieves the < -15 °C dew point over a range of inlet humidity. This means that the inlet effectively *buffers* humidity fluctuations in the inlet. For example, rapid variations in the humidity result in nearly no change in H_2O, while large, long term variations will result in a very slow change in sample water content. Therefore, if there is significant crosstalk between water and C_1, C_2, or C_3, its effect is mitigated because the water level is kept largely constant after passing through the Nafion.

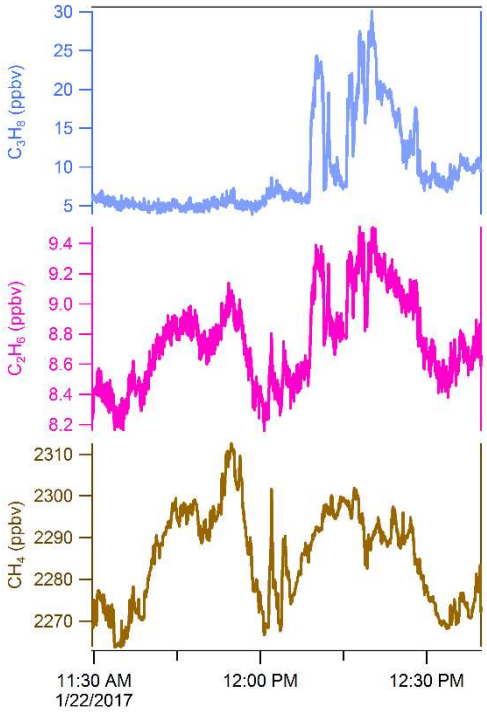

Figure 16. Two plumes from the Aerodyne roof with nearly identical ethane/methane ratios, but very different propane/methane ratios.

5) Field testing of the instrument in a stationary environment

One application of the instrument is fixed-position sampling, e.g. from a roof or tower. To test its applicability under these circumstances, the dual-TILDAS was run in a laboratory at Aerodyne, sampling from an inlet on the building roof. During this sampling, there were two primary types of

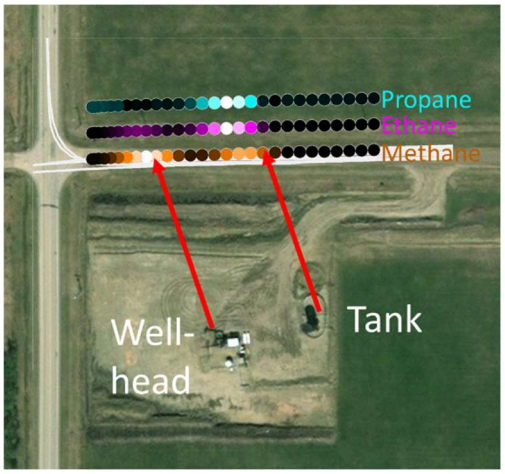

Figure 17. Downwind plume measurement from a typical oil facility. The wellhead (western plume) shows mostly methane, while the tank (eastern plume) shown a large propane and ethane content.

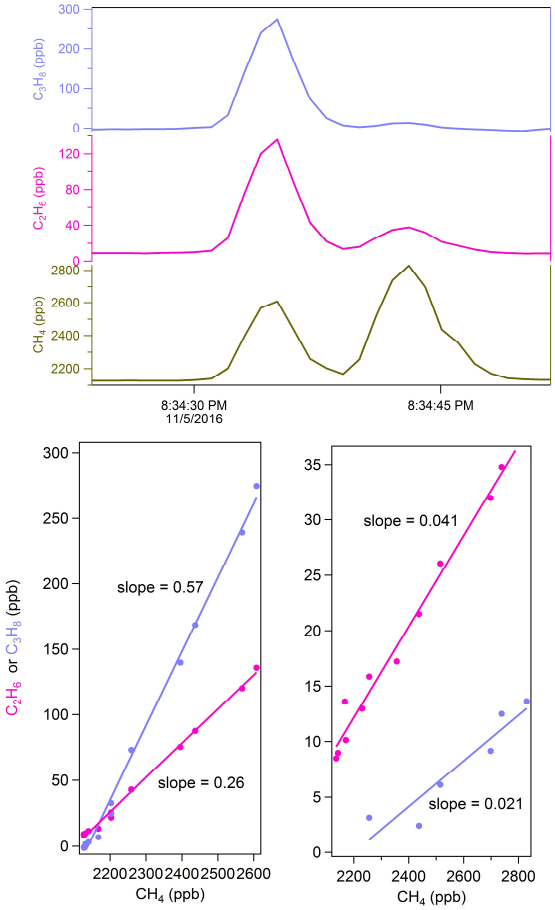

Figure 18. Time series and correlation plots of the plumes in Figure 17. Increasing time in the time series corresponds to movement from east to west (first plume is eastern, tank plume; second plume is western, wellhead plume).

measurement – ambient quantification and plume identification. Shown in Figure 15 is an example of both of those scenarios – a long term variation of methane, ethane, and propane, with fast plumes punctuating the enhancement. Correlation plots of propane vs methane and ethane vs methane (right panel) show an important advantage of the propane measurements. While the propane vs methane correlation clearly shows two ratios – an ambient C_3H_8/CH_4 ratio of 0.13 and plumes with C_3H_8/CH_4 ratios of 1.8 – it would not be clear from the C_2H_6/CH_4 plot that these emissions profiles are from different sources. In this case, the individual fast plumes are likely due to nearby liquefied petroleum gas (LPG) leaks to the northwest of Aerodyne. Concurrent measurements of CO and CO_2 on the roof indicate that there is combustion associated with the plumes, suggesting either a significant leak near an operating LPG combustor, or fuel slip through the combustor.

As another example, Figure 16 shows two plumes, both with similar ethane/methane ratios. If only ethane and methane were being monitored, it would be straightforward to conclude that both plumes are from the same source. However, the first plume contains no propane, while the second plume contains a large amount of propane, indicating two different sources. From a source attribution perspective, these two emitters are clearly different, and without a propane measurement may have been attributed to the same source.

6) Field testing of the instrument aboard a mobile laboratory

The intended purpose of this instrument is to be deployed aboard mobile platforms. Since Aerodyne routinely performs field measurements of oil and gas facilities, the prototype was brought to the field (Alberta, Canada, December 2016) as

part of a campaign aimed at measuring methane emissions in this province. During these studies, clear identification of emissions from different sources was achieved by leveraging the all three measurements. Shown in Figure 17 is an overlay of a pair of plumes intercepted while passing an oil pad east to west (right to left), overlaid on a satellite image. Of the two plumes, the first contains large amounts of propane, while the second contains almost none. The time series of the plumes is shown in the upper panel of Figure 18. As can be seen from the correlations plots in the lower panel, for the first plume the propane/methane ratio is 0.57, while for the second plume it is 0.021. Based upon this data, it appears that the pumpjack emits approximately 60% of total methane coming from the site, and the tank emits ~40%.

Of particular interest in this deployment was to understand the role of external forces on the instrument response. This "motion sickness" is endemic to many sensors, and it is important here to quantify that effect so that we may mitigate it in the prototype stage. Figure 19 shows propane, ethane, and methane while driving. At 8:14:30 pm, the mobile laboratory turned, resulting in a negative value of propane. The ethane measurement was largely unchanged, while any motion sickness in the methane measurement was masked by ambient fluctuations. The propane measurement exhibits significant motion sickness. Inspection of the spectrum shows that the laser light baseline is fluctuating during the turn. Because the propane absorption is so broad, these similarly broad baseline motions intefere with the propane fitting algorithm, resulting in large mixing ratio variations. By comparison, the ethane and methane features are much narrow than the baseline structure, making them more immune to the motion sickness.

To further explore the extent of the motion sickness, the instrument was placed on a suspended platform in the laboratory that was capable of tilting >45° forward, backward, left and right, and had a 3-axis accelerometer mounted aboard. This tilting induces forces perpendicular to the vertical axis of the instrument. As shown in Figure 20, when the instrument is tilted forward and backward (tipped by lifting the front or rear edge), the mixing ratio effect is minor. However, when the instrument is tilted left or right, experiencing lateral forces of ±0.4 g, the effect on propane is dramatic – a ~20 ppb change in mixing ratio. This corresponds to a 50 ppb/g effect on the propane mixing ratio. The ethane and methane force dependences are comparitively small: <2 ppb/g.

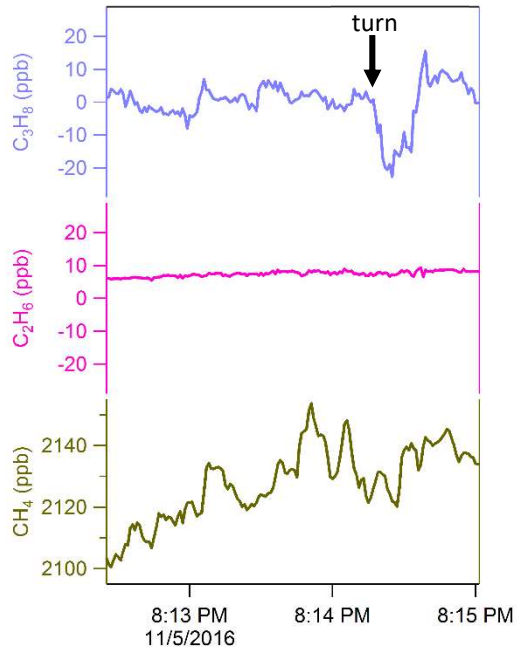

Figure 19. "Motion sickness"' of the instrument in motion aboard the Aerodyne mobile laboratory.

Developing ways to mitigate this effect is going to be a major part of the phase II efforts. There are many possible approaches to attack the problem. The most simple is to harden the optical mount structures to minimize flexing under stress. While we

intend to pursue this, another option is to try to actively compensate for the motion using an optical feedback approach with a fast-motion optical mount. Finally, a third option is to rapidly, mechanically "wobble" the laser beam, washing out the effects of small changes in the beam due to external forces.

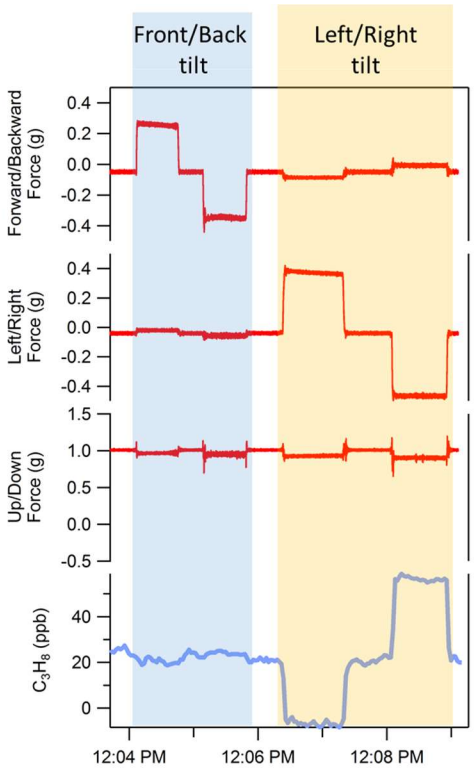

Figure 20. Dependence of propane (lower, blue trace) as a function of front/back tilt (blue shaded), and left/right tilt (yellow shaded).

Task III: Reducing Power and Size Footprint

While the proposed monitor could be used in a laboratory or fixed-station deployment, the intended application is towards a mobile platform. For it to be integrated into existing industry infrastructure, it needs a small, easily deployable footprint. For this development we have two separable goals: reducing the electrical load of the instrument, discussed below, and reducing its size, discussed in Task IV.

The electrical load reduction is achieved by reducing both the pumping and cooling requirements.

Pumping

Typically, TILDAS instruments are best operated with the absorption cell at low pressures, such as 30 Torr. However, because of the broad absorptions associated with ethane and propane, the C_1-C_3 monitor is capable of running at a much higher pressure, as discussed above. This means that the pumping requirements are much lower for this instrument than for a typical TILDAS. In this case, the typical Agilent Triscroll 600 or SH110 scroll pump can be replaced by an Agilent IDP3 scroll pump. This can run at 60 LPM, while drawing only 130 W, as compared to 200 W for the SH110 or 760 W for the Triscroll 600. Conversion to the IDP3 was readily performed without issue, and it was capable of maintaining pressures anywhere from 30-250 Torr in the cell at 1 SLPM operation.

Cooling

Reducing the cooling load is a more difficult problem than the pumping load. Our standard cooling approach is to use a SSCooling Oasis 3 refrigerated circulating chiller. The cooling fluid (a 25% ethanol in water mixture) travels into the instrument, through cooling plates attached to the optical enclosure (two on the sides, one on the optical board), then passes through the two lasers enclosures in series before returning to the circulator. The system not only removes heat from the relatively inefficient lasers, but also maintains the optical enclosure temperature. By cooling the enclosure followed by the laser(s), transient fluctuations in the cooling water temperature

get buffered by the large thermal mass of the enclosure before going into the laser, which may react poorly to the temperature changes.

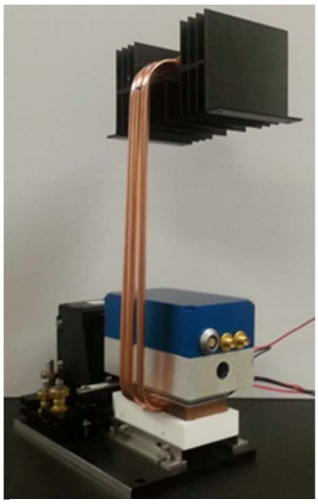

Figure 21. Heat-pump based cooling impementation for interband-cascade lasers.

Prior to the advent of commercially available interband cascade lasers (ICLs), quantum cascade lasers (QCLs) required large amounts of current (100-1000 mA) to operate, and ran between -30 and 10 C), thereby requiring an aggressive cooling approach. ICLs, however, operate at <100 mA and >0 C, allowing a more relaxed cooling scheme. This opens the possibility of using a lower-power cooling system than the Oasis 3, which uses up to 500 W.

We have previously demonstrated the ability to air cool the system using an air-cooled heat pump, an example of which is shown in Figure 21. The blue/silver enclosure contains the laser, which is pointing into the black focusing objective. The problem with this implementation is that it does not allow for the optical enclosure to also be temperature stabilized. This is particularly important for this application, since thermally-induced strain on the optical box as a whole can cause slight misalignments, which result in slow baseline fluctuations that manifest as mixing ratio noise for ethane and propane.

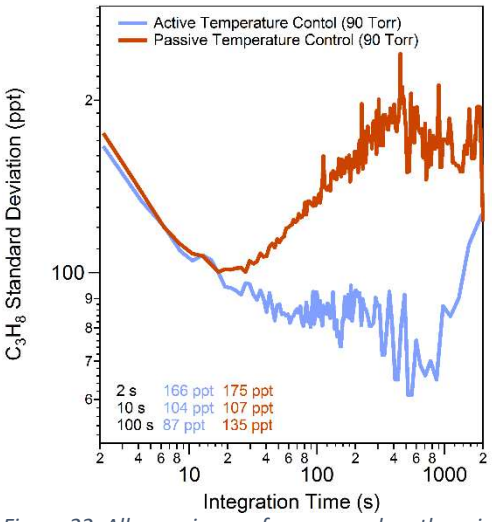

Figure 22. Allan variance of propane when there is no active cooling of the instrument.

To allow for temperature stabilization without the need for aggressive cooling, we demonstrated here that using a circulating fluid without temperature stabilization was a useful approach. In this case, we used the recirculating chiller, but disabled its cooling capacity. The resulting power consumption is ~35 W, a 90% reduction in power consumption. The cooling lines were all insulated, and the instrument temperature initially rose ~5 C to 301 K in the laboratory. This stabilization scheme leverages the large thermal mass of the circulating fluid to buffer temperature changes in the system to a slow enough rate that frequent zeroes (7.5 minutes or 15 minutes) can compensate for the instrument drift. Figure 22 shows the propane profile while sampling from a re-humidified compressed air stream, where the 2-second noise is 175 ppt using the un-chilled circulating fluid. It averages down reasonably well beyond 10 seconds (107 ppt in 10 s), making this type of measurement especially useful for fast plume-based measurements such as those aboard a mobile platform. Over the course of that measurement, the laboratory temperature variation resulted in a 0.3 °C change in instrument temperature, and a rate of change of 0.15 °C/hr.

During phase II we plan on further improving this cooling scheme, specifically looking to allow for some heat release through heat sinks, ways to better insulate the enclosure, and ways to decouple outside thermal changes with deformations on the optical table. In addition, for this phase I testing, an Oasis brand chiller was used with the cooling disabled. During phase II we will explore other pumping options. For example, small continuous-duty water pumps, typically used for fountains and fish tanks, can use as little at 50 W and are designed to be rugged and reliable.

Task IV: Phase II Instrument Design

Phase II funding will be required to develop the prototype into a commercially viable product. Several major tasks need to be completed during phase II:

1) Develop the overall instrument structure
2) Explore other pump options and integrate dryer into pumping system
3) Software improvements

1) Develop overall instrument structure

There will be two products as a result of this project. First, the primary product will be compact, with a small spatial and electrical footprint, aimed toward the oil and gas industry market. However, it needs to control two lasers, a task typically tackled by the Aerodyne dual-TILDAS product line. With the aid of DOE funding, we have recently developed a prototype 2-laser system that is in the same form factor as our compact TILDAS-mini. This compact dual-TILDAS, shown in Figure 23, will serve as the base design for the C_1-C_3 monitor developed during phase II. The instrument contains the same general layout as full dual-TILDAS, but has a reduced laser and collecting objective system, as well as a smaller 76-m cell.

In addition to the primary product of phase II development, a secondary product will be directed toward the research market, where sensitivity will be preferred over mobility. This will be a full dual-TILDAS, shown in Figure 24, which is capable of using an absorption "supercell". Our existing supercell is equivalent to a 204 meter path length. However, we have recently developed a 408 meter multipass cell. The reflecting spot patterns on the rear mirror of the 204 and 408 meter cells are shown in Figure 24. The more compact spot pattern requires a very stable optical alignment entering the cell. This will require the full temperature regulation capabilities of a refrigerated bath, and possibly enhanced insulation. We will also be exploring other laser-objective configurations. Because of the more

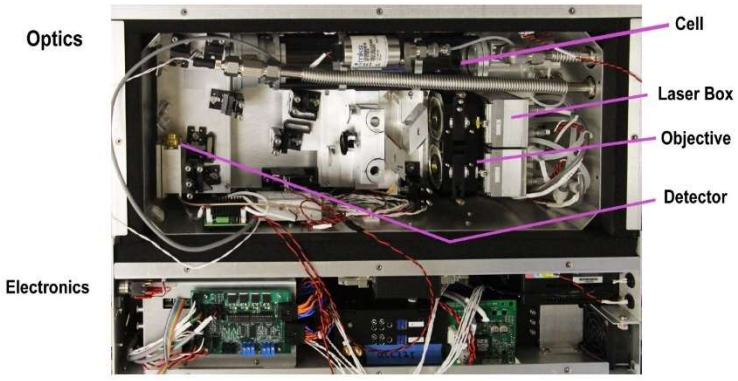

Figure 23. Prototype layout of the compact dual-TILDAS.

compact design of the laser-objective configuration in the compact dual-TILDAS, it may be less susceptible to external vibration and misalignment due to temperature fluctuations.

For both design directions, we plan to use the existing lasers used in the prototype, but will be working with Nanoplus to source even lower-power and higher-temperature ICL lasers. The latest ICLs require such low currents (5-50 mA), we will work with Wavelength Electronics, Inc. to develop very low-current drivers, in an effort to reduce frequency noise on the laser output. This will improve noise on the strong, narrow CH_4 transitions that are artificially broadened by this frequency noise.

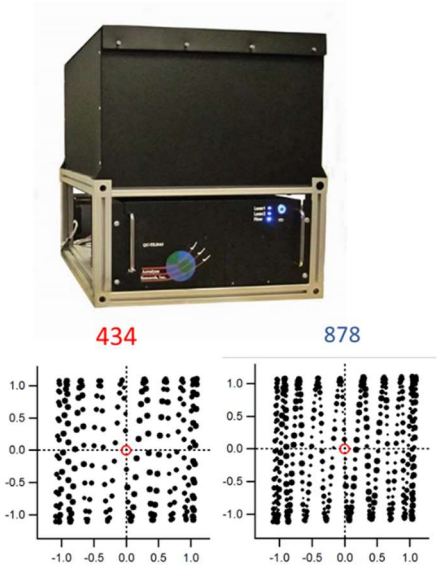

Figure 24. Top: full dual-TILDAS spectrometer, capable of operating two lasers, and using a high pass absorption cell ("supercell"). Bottom: comparison between alignment patterns at 434 passes (left, 200 m, previous state-of-the-art) and at 878 passes (right, 400 m) for the absorption "supercell". The size of the spot decreases proportionally to the pass number to simulate the observed decrease in intensity of the red laser used during the alignment process. The incoming and outgoing beam enter and exit through the cell aperture (red circle).

2) Explore other pump and cooling options and integrate dryer into pumping system

The compact instrument will require a small pump. While the IDP-3 worked well in this application, we will explore other low-power pump options as well. Despite the absorption cell being at elevated pressure (>200 Torr), there is still incentive to have the ability to pull lower pressures in order to achieve the best drying possible from the Nafion dryer. There will be a compromise to balance low power consumption with the dryer performance.

We will also integrate the drying system into the instrument itself. The existing dryer is 24" long and ~2" diameter with Swagelok fittings on each end. An aluminum structure will be built around the compact instrument, with room for the dryer to be mounted within the rack.

Because the goal is for this monitor to be used in leak detection programs for the oil and gas industry, we will aim to reduce the complexity of the plumbing and electrical systems. The pump will still be excluded from the instrument body, in the event that the operator wants to minimize noise or heat load. The plumbing and electrical will consist of simple connections in and out. We will explore liquid and air cooling systems for handling the thermal load, and if the liquid system is preferred, the related pump and fluid reservoir will be enclosed within the monitor rack. Ideally the user will not need to interface with the cooling except to maintain the fluid level. The electrical will be easily accessible for plugging into a car alternator/inverter system.

3) Software Improvements

The end-user of the compact system will benefit from a simple software interface. We

will develop software as a part of TDLWintel that will automate start and maintain the system. Much of this has already been incorporated, but will be modified as needed to readily inform the user when the instrument is warmed up and ready to use. The instrument will also make use of recent advancements in data acquisition software that will couple the output of TDLWintel to optional wind measurements, to provide the end user with the ability to see a time series of recent data alongside the recent wind information to aid in identifying where a plume is coming from. This will be developed in the Igor Pro graphing and programming interface.

Finally, as a part of this system we will provide ethane/methane and propane/methane ratios for plumes, visible to the user in real time. In addition to reading out mixing ratios, this will require plume identification on-the-fly, and associate the higher hydrocarbon ratios each plume. This information will be visible to the driver or a passenger for rapid identification of qualitatively large leak vectors.

References

1. *Annual Energy Outlook 2015*, 2015, Energy Information Administration.
2. *IPCC Fourth Assessment Report: Climate Change 2007; 2.10.2 Direct Global Warming Potentials*, 2007, Intergovernmental Panel on Climate Change.
3. *Energy and Climate Change: World Energy Outlook Special Report*, International Energy Agency.
4. Harrison, M.R., et al., *Methane Emissions from the Natural Gas Industry, Volumes 1 – 15, Final Report, GRI-94/0257 and EPA-600/R-96-080*, 1996, EPA,GRI.
5. Allen, D.T., et al., *Measurements of methane emissions at natural gas production sites in the United States.* Proc. Nat. Acad. Sci., 2013. **110**(44): p. 17768-17773.
6. Subramanian, R., et al., *Methane Emissions from Natural Gas Compressor Stations in the Transmission and Storage Sector: Measurements and Comparisons with the EPA Greenhouse Gas Reporting Program Protocol.* Environ. Sci. Technol., 2014. **49**: p. 3252-3261.
7. Mitchell, A.L., et al., *Measurements of Methane Emissions from Natural Gas Gathering Facilities and Processing Plants: Measurement Results.* Environmental Science & Technology, 2015. **49**: p. 3219-3227.
8. Roscioli, J.R., et al., *Measurements of methane emissions from natural gas gathering facilities and processing plants: measurement methods.* Atmos. Meas. Tech., 2015. **8**(5): p. 2017-2035.
9. Yacovitch, T.I., et al., *Demonstration of an Ethane Spectrometer for Methane Source Identification.* Environmental Science & Technology, 2014. **48**(14): p. 8028-8034.
10. Harrison, J.J. and P. Bernath, *Infrared absorption cross sections for propane (C3H8) in the 3 um region.* J. Quant. Spec. & Rad. Trans., 2010. **111**: p. 1282-1288.
11. Harrison, J.J., N.D.C. Allen, and P.F. Bernath, *Infrared absorption cross sections for ethane (C2H6) in the 3 μm region.* Journal of Quantitative Spectroscopy and Radiative Transfer, 2010. **111**(3): p. 357-363.

12. Rothman, L., et al., *The HITRAN database: 2012 edition.* J Quant Spectrosc Radiat Transfer, 2013.
13. Yang, R.Q., et al., *Continuous-wave operation of distributed feedback interband cascade lasers.* Appl. Phys. Lett., 2004. **84**: p. 3699-3701.
14. Nahle, L., et al., *Interband Cascade Lasers: ICLs open opportunities for mid-IR sensing*, in *Laser Focus World*2013.
15. McManus, J.B., M.S. Zahniser, and D.D. Nelson, *Dual quantum cascade laser trace gas instrument with astigmatic Herriott cell at high pass number.* Applied Optics, 2011. **50**(4): p. A74-A85.
16. Welp, L.R., et al., *Design and performance of a Nafion dryer for continuous operation at CO2 and CH4 air monitoring sites.* Atmos. Meas. Tech., 2013. **6**(5): p. 1217-1226.